

ISOLATION AND NMR CHARACTERIZATION OF 3 β -HYDROXYHOPAN-13(12),22(29)-DIENE AND LUP-20(29)-EN-3-OL,3-HEXENOATE FROM *COMBRETUM GRANDIFLORUM* ROOT BARK AND MOLECULAR DOCKING EVALUATION OF THEIR ANTIMICROBIAL POTENTIAL

*¹Rukayya Muhammed Obansa, ¹George Ileogbulam Ndukwe, ¹Racheal Gbekele-Oluwa Ayo, ¹James Dama Habila, ²Jimoh Tajudeen Abdullahi and ³Uttu Ahmed Jibril

¹Ahmadu Bello University, Zaria, Kaduna State, Nigeria.

²Al-Qalam University, Katsina, Katsina State, Nigeria.

³Federal University, Gashua, Yobe State, Nigeria.

*Corresponding authors' email: obansarukayya@gmail.com

ABSTRACT

Triterpenoids have shown various pharmacological effects, including antimicrobial, anticancer, and cardioprotective activities. *Combretum grandiflorum* has been traditionally used for its antioxidative and antimicrobial properties, however, its root bark remains underexplored as a source of bioactive compounds. This study, therefore, focused on isolating bioactive triterpenoids from *Combretum grandiflorum* root bark extract and assessing their antimicrobial potential. The powdered root bark was subjected to cold maceration using methanol as solvent and polarity dependent fractionation resulted to ethyl acetate fraction. The fraction was subjected to column chromatography, further purification led to the isolation of two compounds. Structural analysis of the compounds was conducted using Nuclear Magnetic Resonance (NMR) spectroscopy, and the results aligned with literature reports. This marks the first report of 3 β -hydroxyHopan-13(12),22(29)-diene and Lup-20(29)-en-3-ol,3-hexenoate from *C. grandiflorum*. The antimicrobial potential of these compounds was further assessed using molecular docking approaches against *Escherichia coli* murein tripeptide amidase (PDB: 5HXD) and *Candida albicans* glutamate dehydrogenase (PDB: 7F77) which are critical for pathogen survival. Molecular docking simulations showed that compound 1 bound to *Escherichia coli* (PDB: 5HXD) and *Candida albicans* (PDB: 7F77) with binding energies of –8.8 and –7.6 kcal/mol, respectively. Compound 2 demonstrated affinities of –8.0 kcal/mol (*E. coli*) and –9.3 kcal/mol (*C. albicans*). This study confirms the presence 3 β -hydroxyHopan-13(12),22(29)-diene and Lup-20(29)-en-3-ol,3-hexenoate triterpenoids in *C. grandiflorum* root bark and highlights their strong *in silico* interactions with microbial targets. These results suggest promising antimicrobial potential and warrant further *in vitro* and *in vivo* studies to experimentally validate their efficacy.

Keywords: Isolation, *Combretum grandiflorum*, 3 β -hydroxyHopan-13(12), 22(29)-diene, Lup-20(29)-en-3-ol,3-hexenoate, Docking studies, *Candida albicans*, *Escherichia coli*, Molecular docking

INTRODUCTION

Medicinal plants have proven since ancient time to have the potential for curing illnesses. The potential for development of therapeutic drugs from plant-derived compounds is immense (Sasidharan *et al.* 2011, Uttu *et al.*, 2022). Worldwide, plants are found, and their various parts including roots, leaves, fruit, stems and flowers, are utilized for many reasons, including medicinal ones (Madumelu *et al.*, 2022). The secondary metabolites isolated from plants have been the main source of novel drugs that bears valuable therapeutic activities (Jimoh *et al.*, 2023). These metabolites include terpenoids, alkaloids, and flavonoids and have been linked to the therapeutic potential of such plants (Iyun *et al.*, 2022).

Combretum grandiflorum (Figure 1) belongs to the *Combretaceae* family. The plant is a climbing shrub native to African countries, including Nigeria. It is a shrub that grows to 6-7 m in height and is found mostly in evergreen forests. The flowers are scarlet in dense spikes and make the plant worthy of cultivation (Burkill, 1985).

Over time, studies on the biological activity of different types of terpenoids have been conducted to find phytochemicals with antibacterial activity for pharmacological application

(Ibrahim *et al.*, 2021, Uttu *et al.*, 2023B). Bacteria such as *Escherichia coli* and *Candida albicans* are known to cause various microbial diseases in humans. *E. Coli* which is a Gram-negative bacterium capable of causing severe food poisoning in humans while the opportunistic pathogenic yeast *Candida albicans* is the cause of candidiasis (Tenailon *et al.*, 2016, Sallau *et al.*, 2022).

Numerous techniques, including *in silico*, *in vitro* and *in vivo* methodologies, have been used to investigate the antibacterial activity of natural plant components. The *in silico* is a recent term that refers to computer-based experimentation that is widely used in today's drug evaluations (Emmanuel *et al.*, 2015, Uttu *et al.*, 2023A). Plants of the *Combretaceae* family have recently been subjected to various chromatographic methods, which have resulted in the isolation of numerous natural compounds with various biological activities. In this study, two terpenoid compound, 3 β -hydroxyHopan-13(12),22(29)-diene (1) and Lup-20(29)-en-3-ol,3-hexenoate (2), were isolated from the ethylacetate extract *C. grandiflorum* root bark. These compounds were characterized using spectral techniques.



Figure 1: Combretum Grandiflorum Showing Leaves and Flowers

MATERIALS AND METHODS

General Experimental Procedures

Collection of Plant Material

The plant sample comprising of the root bark of *Combretum grandiflorum* was collected in Sabon Gari, Kaduna State, Nigeria, identified in September, 2020. It was authenticated in the Herbarium Unit, Department of Botany, Ahmadu Bello University, Zaria, and a herbarium voucher number (V/N): ABU01046 was deposited. The root bark was air dried and pulverized.

Extraction

The pulverized root bark of *C. grandiflorum* (1.5 kg) was macerated with methanol with occasional shaking for 3 days. The extract was filtered and the solvent was removed using rotatory vacuum evaporator under pressure at 40 °C to afford the methanol extract, and sequentially partitioned into dichloromethane and ethyl acetate.

Isolation and Purification

The ethylacetate extract was selected for further studies. Thin-layer chromatography of the ethylacetate extract using multiple solvent systems revealed several spots, with varying retardation factor (R_f). Afterwards, the extract (21.9 g) was pre-adsorbed with 60–120 mesh silica gel and dried. Upon parking (with HEX and silica gel), the dried pre-adsorbed extract was placed on a standard column (5 × 60 cm column) and eluted using a stepwise n-hexane:ethylacetate (HEX:EA) gradient (100:0→0:100, v/v) at a flow rate of 1 drop/sec, yielding 177 collections (50 mL each). The collection was monitored using pre-coated thin-layer chromatographic (TLC) technique and pooled into 18 sub-fractions ($O^1 - O^{18}$),

10% Tetraoxosulphate (VI) acid was used as spraying reagent for visualization. Fraction O^8 was loaded onto a micro-column and compound **1** with $R_f = 0.82$, yield = 13 mg and compound **2** with $R_f = 0.77$, yield = 11 mg as single spots upon TLC across multiple solvent systems.

Molecular Docking Study

The ligands (Compounds 1-2, Ciprofloxacin, Fluconazole) were docked *in silico* with target receptors (PDB: 5HXD and 7F77) that were retrieved from the Protein Data Bank (www.rcsb.org). The ligands were designed using ChemDraw Professional 16.0. and optimized to two-dimensional (2D) structure using Spartan 20v.1.1/2020. Protein structures were prepared by removing water molecules, adding polar hydrogens, and assigning Gasteiger charges and saved in PDB file format in Discovery Studio Visualizer 2021. Docking was performed using AutoDock Vina integrated within PyRx 0.9.8, with a grid box defined around the active site residues (dimensions: 25 × 25 × 25 Å; exhaustiveness = 8). Each docking run was performed in triplicate to ensure reproducibility, and the lowest binding energy pose was selected for interaction analysis. The docking output and binding energy were displayed to examine protein-ligand interactions in Discovery Studio and results were compared against the reference drugs (Tukur *et al.*, 2022, Uttu *et al.*, 2022). The selected protein structures (PDB: 7F77 and PDB: 5HXD) do not contain native co-crystallized ligands, which limited the use of conventional re-docking validation. These structures were chosen due to their high resolution and relevance to the binding domain of interest, hence, assessment of docking reproducibility using multiple scoring functions.

RESULTS AND DISCUSSION

Table 1: The NMR (400 MHz, $CDCl_3$) Data of 3 β -hydroxyHopan-13(12),22(29)-diene (1)

C	3 β -hydroxyHopan-13(12),22(29)-diene			Literature Data Sousa <i>et al.</i> , 2012	
	1H (ppm)	^{13}C (ppm)	DEPT	1H (ppm)	^{13}C (ppm)
1 α	0.94 (H α)	38.67	CH ₂	0.94(H α)	38.9
1 β	1.68 (H β)	-		1.70(H β)	-
2 α	1.66(H α)	27.97	CH ₂	1.63(H α)	27.5
2 β	1.66(H β)	-		1.63(H β)	
3	5.17	78.99	CH	-	78.4
3-	3.21	-	-OH	3.23	-
OH	-	39.98	C	-	39.0
4	0.69	55.13	CH	0.69	55.3
5	1.39(H α)	18.29	CH ₂	1.40(H α)	18.5
6 α	1.53(H β)	-		1.53(H β)	-
6 β	1.42(H α)	33.33	CH ₂	1.47(H α)	33.4

C	<i>3β-hydroxyHopan-13(12),22(29)-diene</i>			Literature Data Sousa et al., 2012	
	¹ H (ppm)	¹³ C (ppm)	DEPT	¹ H (ppm)	¹³ C (ppm)
7 α	1.60(H β)	-		1.62(H β)	-
7 β	-	41.68	C	-	41.7
8	1.25	50.40	CH	1.24	50.4
9	-	37.14	C	-	37.2
10	1.53(H α)	20.90	CH ₂	1.51(H α)	21.1
11 α	1.32(H β)	-		1.32(H β)	-
11 β	1.47(H α)	23.68	CH ₂	1.43(H α)	24.0
12 α	1.47(H β)	-		1.49(H β)	-
12 β	1.36(H β)	48.26	CH	1.37(H β)	49.5
13	-	42.80	C	-	42.1
14	1.39(H α)	34.24	CH ₂	1.42(H α)	33.7
15 α	1.25(H β)	-		1.24(H β)	-
15 β	1.76(H α)	22.69	CH ₂	1.74(H α)	21.7
16 α	1.68(β)	-		1.65(H β)	-
16 β	1.39(H β)	55.25	CH	1.39(H β)	54.9
17 β	-	42.98	C	-	44.8
18	1.57(H α)	40.79	CH ₂	1.60(H α)	41.9
19 α	1.03(H β)	-		1.04(H β)	-
19 β	1.87(H α)	27.38	CH ₂	1.84(H α)	27.4
20 α	1.91(H β)	-		1.97(H β)	-
20 β	2.37 (H β)	46.79	CH	2.67(H β)	46.5
21	-	150.98	C	-	148.6
22	1.02	28.39	CH ₃	1.02	28.2
23	0.79	15.95	CH ₃	0.81	15.97
24	0.83	16.78	CH ₃	0.83	16.7
25	0.94	15.58	CH ₃	0.94	15.9
26	0.97	16.78	CH ₃	0.97	16.7
27	0.76	16.11	CH ₃	0.73	16.1
28	4.69	109.31	CH ₂	4.79	110.2
29	1.76	25.10	CH ₃	1.75	25.0

Table 2: The NMR (400 MHz, CDCl₃) Data of *Lup-20(29)-en-3-ol,3-hexenoate (2)*

C	<i>Lup-20(29)-en-3-ol,3-hexenoate</i>			Literature Data Ekalu 2021	
	¹ H (ppm)	¹³ C (ppm)	DEPT	¹ H (ppm)	¹³ C (ppm)
1 α	1.62	38.73	CH ₂	1.6 m	38.6
1 β	1.62	-		1.65 m	-
2 α	2.01	27.87	CH ₂	2.01 m	27.4
2 β	2.01	-		2.01 m	
3	5.00	79.02	CH	4.48 dd	80.8
4	-	39.24	C	-	39.6
5	0.77	55.17	CH	0.79 m	55.6
6	0.76	18.29	CH ₂	18.4	0.75 m
7	1.76	38.3	CH ₂	1.65 m	38.3
8	-	41.62	C	-	41.1
9	1.25	50.08	CH	1.28 d	50.6
10	-	37.57	C	-	37.3
11 α	0.92	22.95	CH ₂	0.86 d	22.9
11 β	0.92	-		-	-
12 α	1.62	25.90	CH ₂	1.62 m	25.4
12 β	1.62	-		1.62 m	-
13	-	38.12	CH	-	38.1
14	-	43.15	C	-	43.2
15 α	1.98	27.65	CH ₂	2.00 m	27.6
15 β	1.98	-		2.00 m	-
16 α	1.62	32.40	CH ₂	1.62 m	32.1
16 β	1.62	-		1.62 m	-
17	-	43.18	C	-	43.2
18	2.32	47.59	CH	2.38 m	48.5

C	<i>Lup-20(29)-en-3-ol,3-hexenoate</i>			Literature Data Ekalu 2021	
	¹ H (ppm)	¹³ C (ppm)	DEPT	¹ H (ppm)	¹³ C (ppm)
19	1.37	47.03	CH	1.35 m	48.2
20	-	150.05	C	-	151.2
21 α	1.25	25.90	CH ₂	1.26 m	25.3
21 β	1.25	-		1.26 m	1
22 α	1.39	41.02	CH ₂	1.38 m	40.2
22 β	1.39	-	-	1.38 m	-
23	1.59	28.07	CH ₃	1.59 s	28.2
24	0.90	17.01	CH ₃	0.84 s	16.2
25	1.07	17.61	CH ₃	1.02 s	16.4
26	0.67	15.31	CH ₃	0.53 s	14.7
27	0.77	15.08	CH ₃	0.78 s	14.3
28	0.98	18.29	CH ₃	0.89 s	19.5
29 α	5.00	109.89	CH ₂	4.69 d	109.6
29 β	5.00	-		4.57 d	-
30	1.59	18.29	CH ₃	1.59 s	18.2
C-1'	-	172.39	C	-	173.9
C-2'	1.42	30.08	CH ₂	1.46 m	30.01
C-3'	5.28	130.51	CH	5.35 m	130.2
C-4'	5.24	129.75	CH	5.35 m	129.9
C-5	1.37	29.70	CH ₂	1.38-1.43*	29.81
C-6'	0.98	15.08	CH ₃	0.84 m	14.3

Table 3: Docking Results of Compounds with Active site of the Receptor (PDB: 5HXD)

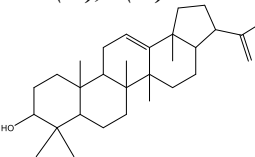
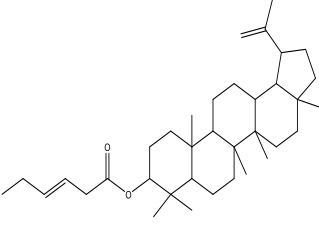
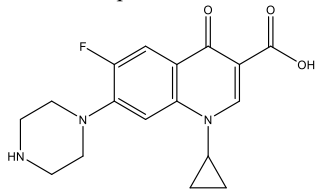
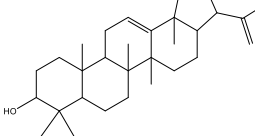
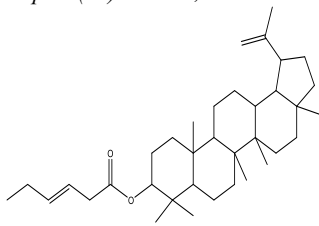
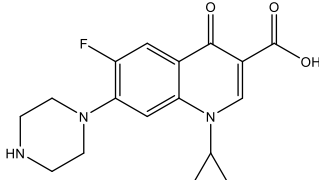
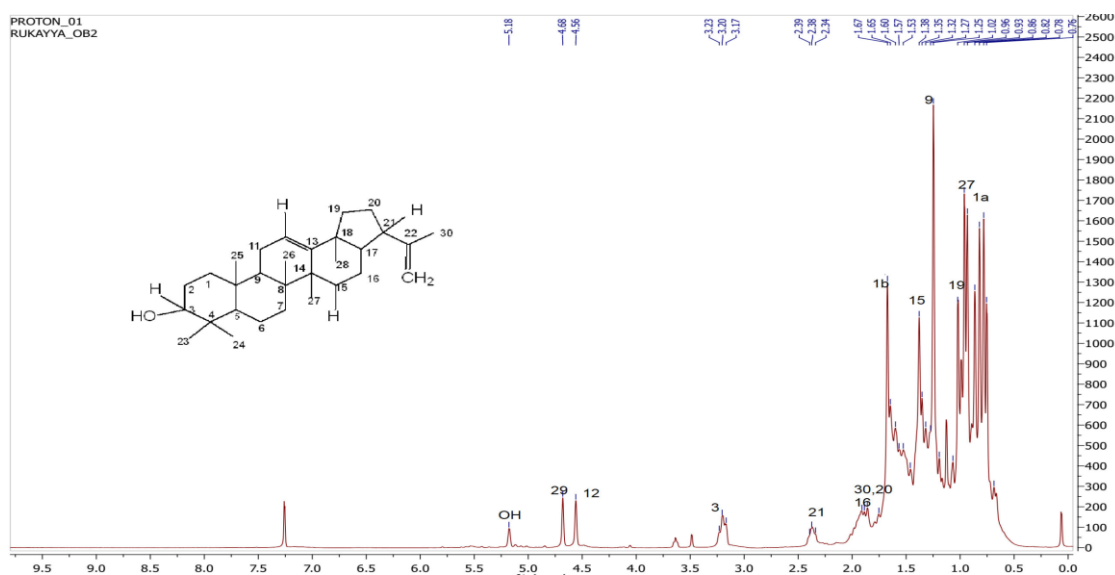
S/N	Ligands	Binding Score (Kcal/mol)	Protein Interaction	Types of Interaction	Bond Distance Å
1	<i>3β-hydroxyHopan-13(12),22(29)-diene</i> 	-8.8	GLU A:164 SER A:186 ILE A:207 THR A:208 CYS A:206 PRO A:166 GLY A:196 SER A:194 THR A:191 SER A:197 ASN A:105 GLU A:190	Van der Waals Van der Waals Van der Waals Van der Waals Van der Waals Van der Waals Van der Waals Van der Waals Van der Waals Van der Waals Van der Waals Van der Waals	5.03 5.06 4.98 4.26 4.77 4.05 4.51 4.30 5.25 2.97 4.97 4.58
2	<i>Lup-20(29)-en-3-ol,3-hexenoate</i> 	-8.0	THR A:208 ASN A:98 HIS A:157 HIS A:49	Conventional Hydrogen Bond Conventional Hydrogen Bond Pi-Alkyl Pi-Alkyl	2.45 1.80 4.80 5.02
3	Ciprofloxacin 	-7.5	ARG A:167 ALA A:200 ALA A:200 ALA A:200 CYS A:206 CYS A:206 PRO A:166 PRO A:166 GLY A:196 GLU A:164	Conventional Hydrogen Bond Pi-Sigma Pi-Alkyl Alkyl Conventional Hydrogen Bond Pi-Sulfur Pi-Alkyl Pi-Alkyl Carbon Hydrogen Bond Carbon Hydrogen Bond	2.07 3.45 4.58 4.20 1.80 5.85 4.05 3.87 3.12 3.61

Table 4: Docking Results of Compounds with Active site of the Receptor (PDB: 7F77)

S/N	Ligands	Binding Score (Kcal/mol)	Protein Interaction	Types of Interaction	Bond Distance Å
1	<i>3β-hydroxyHopan-13(12),22(29)-diene</i> 	-7.6	LYS B:189 PHE B:185 PRO C:95	Alkyl Pi-Alkyl Alkyl	5.13 5.12 5.26
2	<i>Lup-20(29)-en-3-ol,3-hexenoate</i> 	9.3	LYS A:76 LYS A:76 ASP A:75 SEP A:144	Alkyl Alkyl Van der Waals Van der Waals	4.13 5.36 4.07 4.20
3	Fluconazole 	-7.3	GLN B:118 GLY B:98 LYS B:97 GLY B:397 VAL B:398 ALA B:171 ASP B:173 ASN B:250 GLY B:172	Conventional Hydrogen Bond Halogen (Fluorine) Conventional Hydrogen Bond Amide-Pi Stack Pi-Alkyl Pi-Alkyl Conventional Hydrogen Bond Conventional Hydrogen Bond Conventional Hydrogen Bond	2.77 3.37 2.25 4.34 4.34 4.90 2.98 2.83 2.20

**Figure 2: ¹H NMR Spectrum of *3β-hydroxyHopan-13(12),22(29)-Diene* (1)**

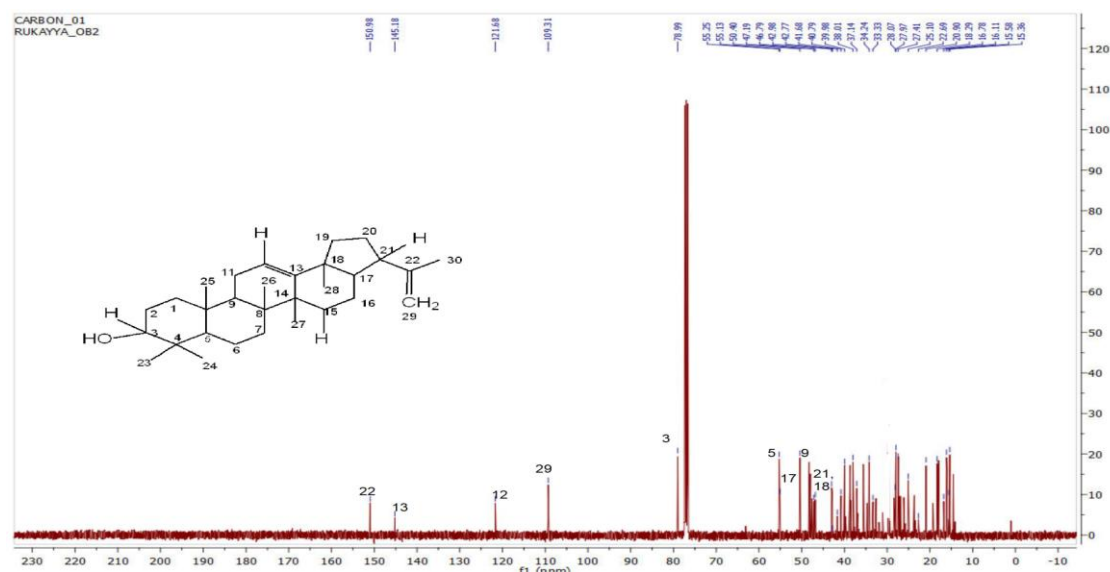


Figure 3: ^{13}C NMR Spectrum of 3β -hydroxyHopan-13(12),22(29)-Diene (1)

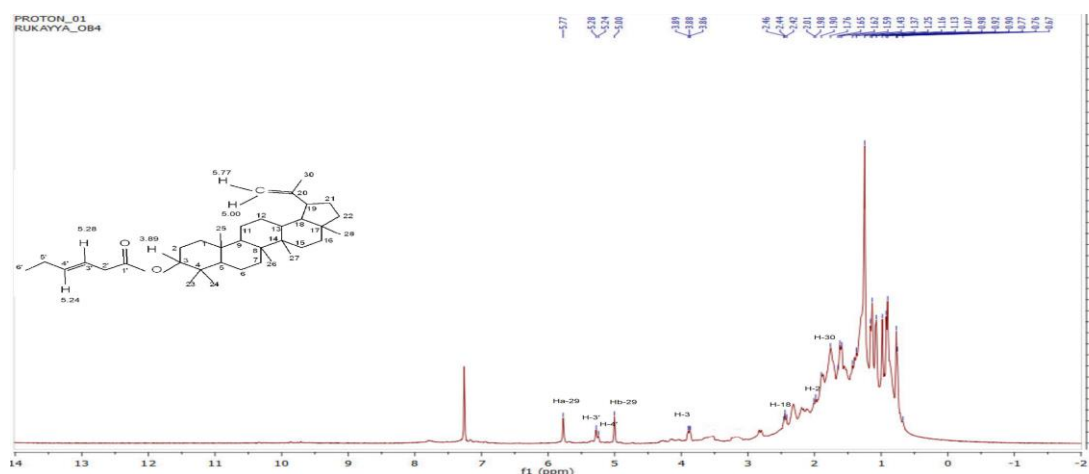


Figure 4: ^1H NMR Spectrum of *Lup-20(29)-en-3-ol,3-Hexenoate* (2)

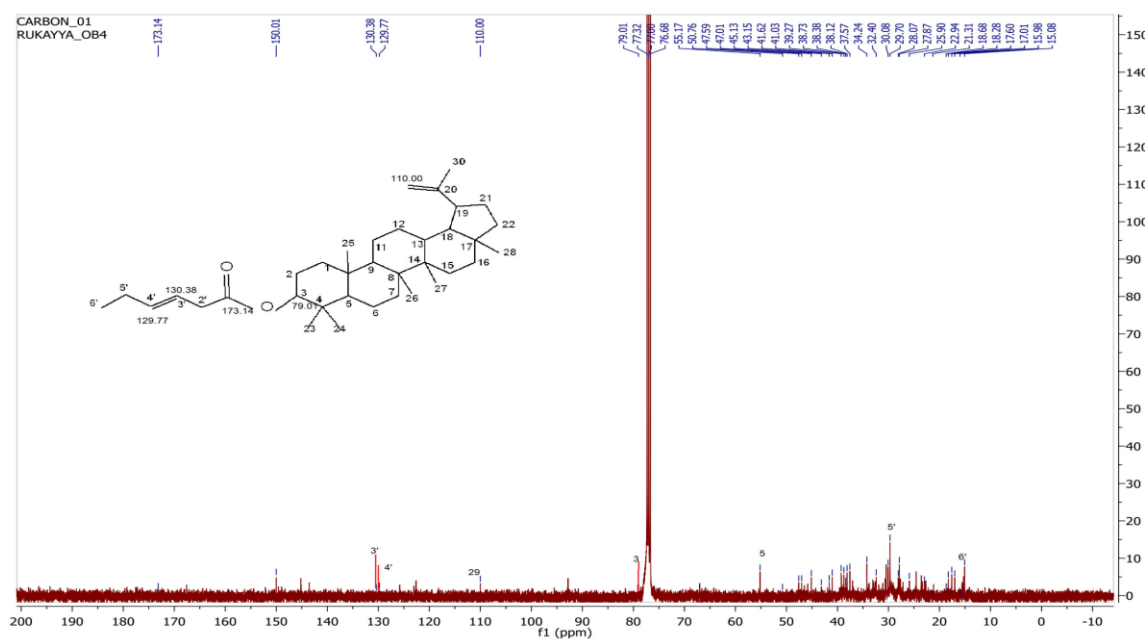
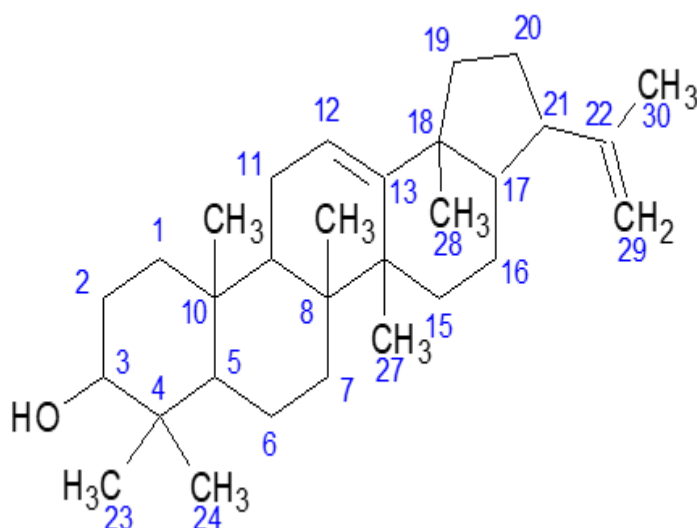
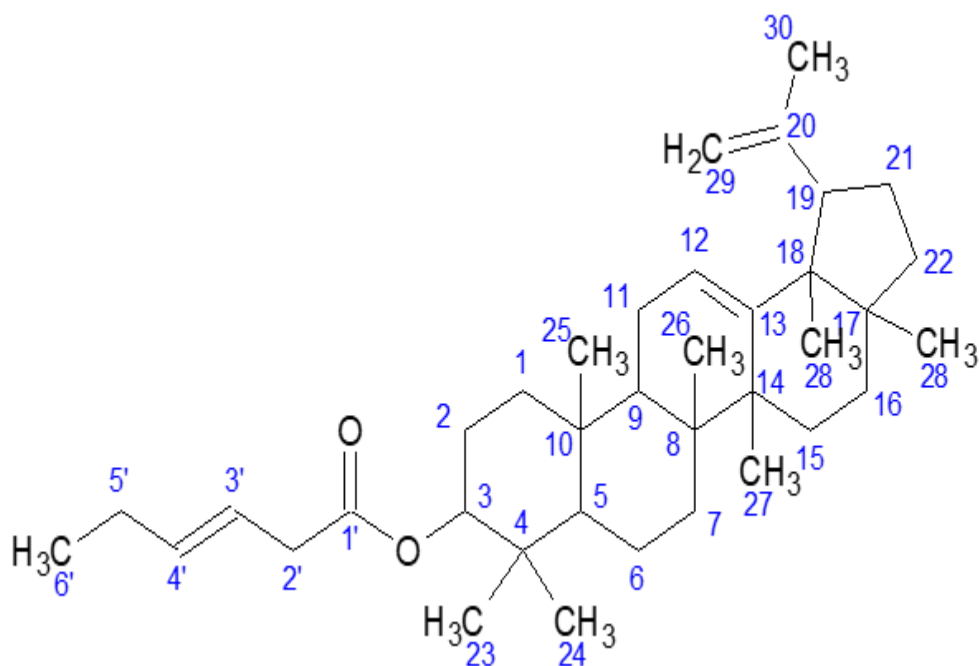
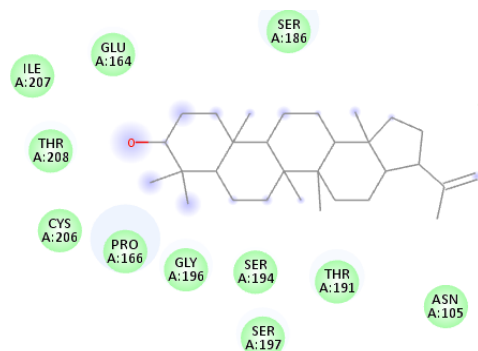
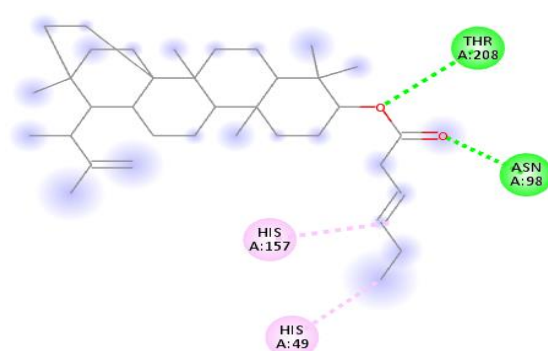


Figure 5: ^{13}C NMR Spectrum of *Lup-20(29)-en-3-ol,3-Hexenoate* (2)

Figure 6: Structure of *3β*-hydroxyHopan-13(12),22(29)-Diene (1)Figure 7: Structure of *Lup-20(29)-en-3-ol,3-Hexenoate* (2)Figure 8: 2D Interaction of *3β*-hydroxyHopan-13(12),22(29)-diene (1) with Crystal Structure of *E. coli* (PDB: 5HXD)Figure 9: 2D Interaction of *Lup-20(29)-en-3-ol,3-hexenoate* (2) with Crystal Structure of *E. coli* (PDB: 5HXD)

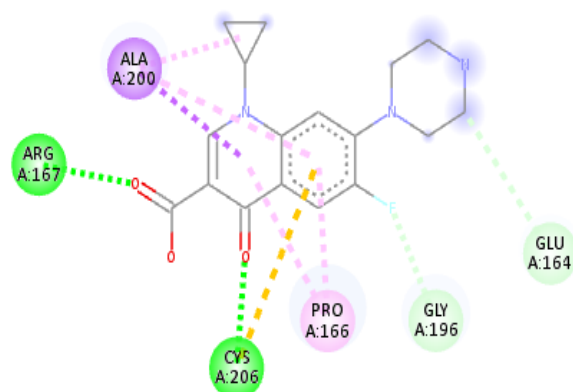


Figure 10: 2D Interaction of Ciprofloxacin with Crystal Structure of *E. coli* (PDB: 5HXD)

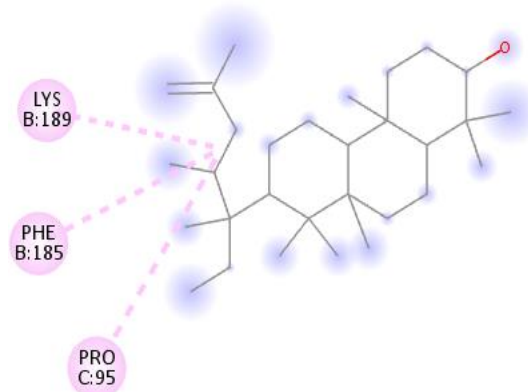


Figure 11: 2D Interaction of 3β -Hydroxyhopan-13(12),22(29)-diene (1) with Crystal Structure of *C. albicans* (PDB: 7F77)

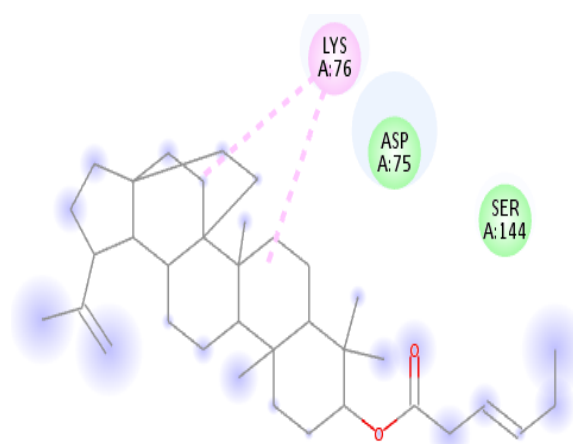


Figure 12: 2D Interaction of *Lup-20(29)-en-3-ol,3-Hexenoate* (2) with Crystal Structure of *C. Albicans* (PDB: 7F77)

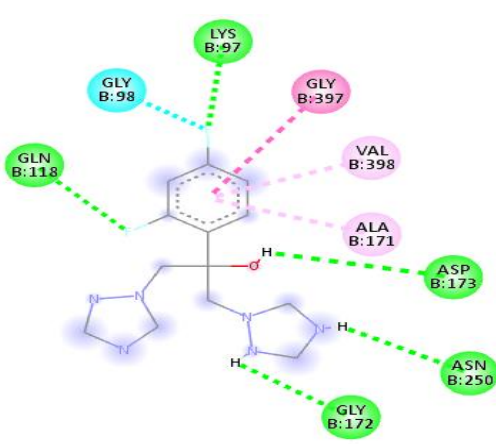


Figure 13: 2D Interaction of Fluconazole with Crystal Structure of *C. Albicans* (PDB: 7F77).

Compound **1** (13 mg), in the form of a white amorphous solid and the nuclear magnetic resonance (NMR) spectra data (Table 1) of compound **1** was very similar to the literature (Sousa *et al.*, 2012) for 3β -hydroxyHopan-13(12),22(29)-diene. The alkenyl hydrogen atoms of a methylenic carbon (C-29) are represented by a signal at δ H 4.68 (H-29, integrating for two hydrogen atoms) in the 1 H-NMR spectrum. There is no hydrogenation of the other alkenyl carbon (C-22). At δ H 3.23, the multiplet is ascribed to carbinolic hydrogen (C-OH, C-3). The signal at δ H 2.37 indicates that hydrogen is adjacent to an alkenyl group (H-21). At δ H 1.76, 1.02, 0.97, 0.94, 0.83, 0.79, and 0.76, the singlets are ascribed to methylic hydrogen atoms, specifically at H-30, H-23, H-27, H-26, H-25, H-24, and H-28.

The 13 C-NMR spectrum displays signals that are typical of an alkenyl group at δ c 150.98, 145.18 (for C-22 and C-13 non-hydrogenated carbon atoms, respectively) and 109.31, 121.68 (for C-29 and C-12 methylenic and methynic carbon atoms, respectively). A carbinolic carbon (C-3) is represented by the signal at δ c 78.91. Five non-hydrogenated (δ c 42.98, 42.77, 41.68, 39.98, and 37.69) and five methynic (δ c 55.25, 55.13, 50.40, 47.19, and 46.79) carbon atoms, ten methylenic (δ c 42.77, 38.01, 34.24, 33.33, 27.97, 27.41, 24.78, 22.37, 20.58, and 18.04), and seven methylic (δ c 28.07, 25.41, 17.67, 15.26, 17.98, 15.63, and 15.79) carbon atoms are also identified in the 13 C-NMR spectrum. The correlated spectroscopy (COSY) contour map of OB2 displays correlations between the signals

at δ H 3.23 (H-3) and δ H 1.63 (H-2); δ H 1.53 (H-6 β) and 1.39 (H-6 α) and δ H 0.69 (H-5); δ H 1.91 (H-20 β) and 1.87 (H-20 α) and δ H 1.57 (H-19 α) and 1.03 (H-19 β); δ H 2.37 (H-21) and the signals at δ H 1.39 (H-17), 1.91 (H-20 β), and 1.87 (H-20 α); δ H 4.68 (H-29) and δ H 2.37 (H-21) and 1.76 (H-30).

On the heteronuclear multiple bond correlation (HMBC) contour map, the hydrogen signal at δ H 3.23 (H-3) correlates with the carbon signals at δ c 39.44 (C-4), 28.07 (C-23), and 15.79 (C-24); the hydrogen signal at δ H 2.37 (H-21) correlates with the carbon signals at 150.66 (C-22), 108.99 (C-29), δ c 54.81 (C-17), 42.66 (C-18), 27.10 (C-20), and 25.41 (C-30); the hydrogen signal at δ H 4.68 (H-29) correlates with the carbon signals at 150.66 (C-22), 46.47 (C-21), and 25.41 (C-30); the hydrogen signal at δ H 1.76 (H-30) correlates with the carbon signals at 150.66 (C-22), 108.99 (C-29), and δ c 46.47 (C-21).

The NMR spectra data (Table 2) of compound **2**, which weighed 11 mg and was a white solid, were very similar to the literature (Ekalu, 2021) for *Lup-20(29)-en-3-ol,3-hexenoate*. The triterpenoid pattern was revealed by the 1 H-NMR spectrum (400 MHz, CDCl_3) (Table 5.2), which included eight methyl signals in the up-field at δ H 0.90 (C-24), 1.06 (C-25), 1.59 (C-23), 0.77 (C-27), and 0.67 (C-26). The single methyl group at position-30 also showed up as a sharp singlet at δ H 1.59 (C-30). There was evidence of a double bond between C-20 and C-29 based on the down-field shift for C-30. A multiplet at δ H 5.24–5.28 (H-3' and H-4') and two broad

singlets at δ H 5.77 (1H, br s, H-29 α) and 5.00 (1H, br s, H-29 β) were found in the down-field region of the spectrum, indicating the presence of olefinic protons.

The HMBC spectrum revealed correlations between the carbon signal at δ C 109.91 and H-29 α at δ H 5.77 (1H, br s) and H-29 β at δ H 5.00 (1H, br s). The presence of 36 carbon signals, representing eight methyl groups and thirteen methylene groups including one connected to a carbonyl carbon that appeared at δ C 30.08 for C-2' were seen in the 13 C-NMR spectrum (400 MHz, CDCl₃). Seven quaternary carbon atoms and eight methine groups, including one connected to oxygen at δ C 79.02 for C-3, were seen. At δ C 150.05 and 109.89, the olefinic carbons C-20 and C-29 were visible, whereas C-3' and C-4' were visible at 130.51 and 129.75, respectively. Correlations between the proton signal at δ H 3.18 (H-3) and the carbon signals at δ C 15.35 (C-24), 27.96 (C-23) and 38.64 (C-1) were found using heteronuclear single quantum coherence (HSQC) and HMBC experiments.

Molecular docking simulations were used to assess how well the isolated compounds fit into the binding pockets of two microbial targets: *Escherichia coli* Mtp amidase (PDB: 5HXD) and *Candida albicans* glutamate dehydrogenase 3 (PDB: 7F77). The binding affinities and types of molecular interactions observed are presented in the results. Compound 1 demonstrated notable binding to the bacterial target, with a binding energy of -8.8 kcal/mol, involving multiple Van der Waals interactions. Compound 2 exhibited a binding score of -8.0 kcal/mol and formed conventional hydrogen bonds, along with Pi-alkyl interactions. Against the fungal target, compound 1 had a score of -7.6 kcal/mol, while compound 2 displayed the strongest binding at -9.3 kcal/mol. Comparatively, ciprofloxacin and fluconazole showed binding affinities of -7.5 kcal/mol and -7.3 kcal/mol, respectively.

Discussion

The compounds *3 β -hydroxyHopan-13(12),22(29)-diene* and *Lup-20(29)-en-3-ol,3-hexenoate* were successfully isolated from *C. grandiflorum* root bark for the first time and structurally elucidated using detailed spectroscopic techniques, in agreement with literature data (Sousa *et al.* 2012, Ekalu, 2021). The docking studies revealed favourable interactions of these triterpenoid compounds with the antimicrobial targets *Escherichia coli* murein tripeptide amidase (PDB: 5HXD) and *Candida albicans* glutamate dehydrogenase 3 (PDB: 7F77) indicating potential mechanisms of antimicrobial action.

The results suggest both compounds have a high binding affinity for the active sites of microbial enzymes associated with *E. coli* and *C. albicans*. For compound 1, the binding was predominantly driven by hydrophobic and Van der Waals interactions.

Compound 2 formed strong hydrogen bonds and additional Pi-alkyl interactions, enhancing its binding strength and specificity.

For *E. coli* (5HXD), compound 1 (*3 β -hydroxyHopan-13(12),22(29)-diene*) primarily engaged in multiple Van der Waals connections with key amino acid residues such as GLU A:164, SER A:186, ILE A:207, and THR A:208. These weak, non-covalent interactions, though individually small in energy contribution, collectively stabilize the ligand within the active site. Notably, SER A:197 formed a Van der Waals contact at a shorter bond distance (2.97 Å), suggesting a closer and possibly more specific interaction. The absence of hydrogen bonding implies that hydrophobic and steric interactions predominantly drive the binding of compound 1,

which aligns with the rigid, hydrocarbon-rich structure of hopane derivatives.

In contrast, compound 2 (*Lup-20(29)-en-3-ol,3-hexenoate*) exhibited conventional hydrogen bonding with THR A:208 and ASN A:98 at close distances (2.45 Å and 1.80 Å, respectively), indicating strong and directional bonding. Additionally, Pi-alkyl interactions with histidine residues (HIS A:157 and HIS A:49) contributed to ligand anchoring within the hydrophobic pockets. These hydrogen bonds are crucial for molecular recognition and binding specificity and are facilitated by the presence of hydroxyl and ester functional groups in compound 2.

In the case of *Candida albicans* (7F77), compound 1 formed hydrophobic (alkyl and Pi-alkyl) interactions with LYS B:189, PHE B:185, and PRO C:95. These interactions suggest that the lipophilic nature of the triterpene allows deep penetration into the hydrophobic core of the fungal enzyme. Compound 2 again showed superior binding, with multiple alkyl interactions (LYS A:76), alongside Van der Waals forces (ASP A:75, SEP A:144), all of which contributed to its notable binding energy of -9.3 kcal/mol. Such interactions indicate good complementarity between the ligand and the protein's hydrophobic pockets.

These molecular insights imply that both compounds can occupy the active sites of bacterial and fungal proteins via a combination of hydrophobic, Van der Waals, hydrogen bonding, and aromatic interactions. This interaction pattern supports their potential as broad-spectrum antimicrobial agents, especially given their comparable or better binding energies than standard drugs like ciprofloxacin and fluconazole. Moreover, the structural rigidity and functional group diversity of the compounds enhance their fit and binding stability within the enzyme cavities.

Nevertheless, docking provides only preliminary evidence of activity. The static nature of docking fails to capture protein flexibility, solvent effects, or metabolic processes, raising risks of false positives. Moreover, strong binding does not guarantee biological efficacy. Experimental validation through enzyme inhibition assays, antimicrobial susceptibility testing, and cytotoxicity profiling is necessary to confirm the predicted activity.

CONCLUSION

In this study, two triterpenoid compounds, *3 β -hydroxyHopan-13(12),22(29)-diene* and *Lup-20(29)-en-3-ol,3-hexenoate* were successfully isolated for the first time from the *C. grandiflorum* root bark ethyl acetate extract and characterized using NMR spectroscopy. *In silico* molecular docking analysis demonstrated favourable interactions between the compounds and microbial enzymes from *E. coli* and *C. albicans*. The binding affinities of these compounds toward *E. coli* and *C. albicans* target enzymes surpassed those of standard antimicrobial agents.

The *in silico* activity of *Lup-20(29)-en-3-ol,3-hexenoate* against microbial target enzymes is consistent with previous reports on the antimicrobial efficacy of structurally related triterpenoids, such as Lupeol acetate (Mukthar *et al.*, 2018) and Lupeol (Ekalu *et al.*, 2019). Similarly, the findings align with observations by Liu *et al.* (2014), who reported strong antimicrobial activity of hopane-type triterpenoids. Together, these comparisons reinforce the likelihood that the observed binding profiles reflect genuine biological relevance.

The docking analysis indicated that compound 1 predominantly interacts via Van der Waals and hydrophobic contacts, whereas compound 2 forms stronger, more specific interactions, including conventional hydrogen bonds and Pi-alkyl interactions. Such interaction patterns suggest

favourable structural and chemical complementarity with microbial target proteins, providing molecular insight into their potential mechanisms of action.

Overall, these results provide compelling preliminary evidence that naturally derived triterpenoids from *C. grandiflorum* may serve as promising antimicrobial candidates. However, as docking studies represent only predictive models, further *in vitro* and *in vivo* investigations are essential to validate these findings, their pharmacokinetic and toxicity profiles be evaluated, and their applicability in drug development should be assessed.

REFERENCES

- Adamu M., Uttu A. J., Ajala A., Obansa R. M. and Madumelu M. (2023). A short review on plants used as anti-snake venom. *Journal of Chemical Reviews*, 5(3), 341–352. <https://doi.org/10.22034/jcr.2023.397955.1221>
- Baffa A. A., Waziri M. and Uttu A. J. (2022). Dietary Intake of Heavy Metals from the Consumption of Fruits and Vegetables in Gashua, Nigeria. Proceedings of the 45th Annual International Conference, Workshop, and Exhibition of the Chemical Society of Nigeria (CSN). Pages 211 – 217
- Burkill H.M. (1985). The useful plants of west tropical Africa, Vol 1
- Ekalu, A., Gbekele-Oluwa, A. R., Habila. J., Hamisu, I. (2019). Bioactivities of Phaeophytin a, α -Amyrin, and lupeol from *Brachystelma togoense* Schltr. *Journal of Turkish Chemical Society A*. 6(3):411–8. <https://doi.org/10.18596/jotcsa.571770>
- Ekalu, A. (2021). Isolation, characterization and antimicrobial activities of bioactive compounds from *Brachystelma togoense* Schltr. (Apocynaceae) and *Strombosia grandifolia* Hook. F. ex. Benth (Olacaceae). PhD Thesis. Pp. 81&201
- Emmanuel I. E*, Uttu A. J., Oluwaseye A., Hassan S. and Ajala A. (2015). A Semi-empirical based QSAR study of indole β - Diketo acid, Diketo acid and Carboxamide Derivatives as potent HIV-1 agent Using Quantum Chemical descriptors. *IOSR Journal of Applied Chemistry*, 8(11i); 12-20. <https://doi.org/10.9790/5736-08111220>
- Gow N. A. and Yadav B. (2017). Microbe Profile: *Candida albicans*: a shape-changing, opportunistic pathogenic fungus of humans. *Microbiology*. 163 (8): 1145-1147. <https://doi.org/10.1099/mic.0.000499>
- Ibrahim H., Uttu A. J., Sallau M.S. and Iyun O. R. A. (2021). Gas chromatography–mass spectrometry (GC–MS) analysis of ethyl acetate root bark extract of *Strychnos innocua* (Delile). *Beni-Suef University Journal of Basic and Applied Sciences*, 10(65); 1-8. <https://doi.org/10.1186/s43088-021-00156-1>
- Iyun O. R. A., Uttu A. J., Sallau M. S. and Ibrahim H. (2022). GC-MS Analysis of Methanol Extract of *Strychnos innocua* (Delile) Root Bark. *Advanced Journal of Chemistry-Section A*, 2022, 5(2), 104-117. DOI: <https://doi.org/10.22034/AJCA.2022.322806.1295>
- Jimoh, T., Tukur, A., Musa, N. M., Obansa, R. M. and Ismail, M. (2023). Phytochemical and Gas Chromatography-Mass Spectrometry (GC-MS) Analysis of Ethyl Acetate Root Extract of *Indigofera diphylla*. *Advanced Journal of Chemistry, Section B: Natural Products and Medical Chemistry*, 5(2), 173-183. doi: 10.22034/ajcb.2023.364179.1127
- Liu, C., Liao, Z. X., Liu, S. J., Ji, L. J., Sun, H. F. (2014). Two new 2,3-seco-hopane triterpene derivatives from *Megacodon stylophorus* and their antiproliferative and antimicrobial activities. *Planta Medica*, 80(11):936-41. doi: 10.1055/s-0034-1368612. Epub 2014 Jul 4. PMID: 24995501.
- Madumelu M., Iwuala N. B. and Uttu, J. A. (2022). Antimicrobial potentials and phytochemical investigation of stem bark methanolic extract and fractions of *Millettia chrysophylla* Dunn. *FUDMA Journal of Sciences*, 6(3), 222 – 225. <https://doi.org/10.33003/fjs-2022-0603-984>
- Muktar, B., Bello, I. A., & Sallau, M. S. (2018). Isolation, characterization and antimicrobial study of *Lup-20(29)-en-3-ol,3-hexenoate* from the root bark of Fig-Mulberry Sycamore (*Ficus sycamorus* LINN). *Journal of Applied Sciences and Environmental Management*, 22(7), 1129-1133.
- Sallau M. S., Uttu A. J., Ibrahim H., Idris A. Y. and Habila J. D. (2016). Isolation of a major antimicrobial compound from stem bark of *Glossonema boveanum* (Decne) *British Biotechnology Journal*, 16(2); 1-10. DOI: <https://doi.org/10.9734/BBJ/2016/24436>
- Sallau M. S., Uttu A. J., Iyun O. R. A. and Ibrahim H. (2022). *Strychnos innocua* (Delile): Phytochemical and Antimicrobial Evaluations of its root bark extracts. *Advanced Journal of Chemistry, Section B*, 4(1), 17-28. DOI: <https://doi.org/10.22034/ajcb.2022.323148.1104>
- Sasidharan S., Chen Y., Saravanan D., Sundram K. M. and Latha L. Y. (2011). Extraction, isolation and characterization of bioactive compounds from plants extracts. *African Journal of Traditional Complementary and Alternative Medicine*, 8(1): 1-10. PMID: 22238476
- Sousa, G. F., Duarte, L. P., Alcantara, A. F. C., Silva, G. D. F., Vieira-Filho, S. A., Silva, R. R., Oliverira, D. M. and Takahashi, J. A. (2012). New triterpenes from *Maytenus robusta*: structural elucidation based on NMR experimental data and theoretical calculations. *Molecules*, 17(11), 13439-13456
- Tenaillon O., Skurnik D., Picard B. and Denamur E. (2010). The population genetics of commensal *Escherichia coli*. *Nature Reviews. Microbiology*. 8 (3): 207–17. <https://doi.org/10.1038/nrmicro2298>
- Tukur A., Habila J. D., Ayo R.G. and Iyun O. R. A. (2022). Design, synthesis, docking studies and antibiotic evaluation (in vitro) of some novel (E)-4-(3-(diphenyl-amino)phenyl)-1-(4-methoxyphenyl)-2-methylbut-3-en-1-one and their analogues. *Bulletin of the National Research Centre*, 46(60), 1-12. <https://doi.org/10.1186/s42269-022-00745-9>
- Uttu A. J., Sallau M. S., Iyun O. R. A. and Ibrahim H. (2022). Recent Advances in Isolation and Antimicrobial Efficacy of Selected *Strychnos* Species: A Mini Review. *Journal of Chemical Reviews*. 4(1), 15-24. <https://doi.org/10.22034/JCR.2022.314381.1129>
- Uttu A. J., Sallau M. S., Ibrahim H. and Iyun O. R. A. (2022). Isolation, characterization, and docking studies of

campesterol and β -sitosterol from *Strychnos innocua* (Delile) root bark, *Journal of Taibah University Medical Sciences*, 18(3): 566-578. <https://doi.org/10.1016/j.jtumed.2022.12.003>

Uttu A. J., Sallau M.S., Ibrahim H. and Iyun O.R.A. (2023A). *In silico* modelling and NMR Characterization of some steroids from *Strychnos innocua* (Delile) root bark as

potential antifungal agents. *Steroids*, 194, 109222. <https://doi.org/10.1016/j.steroids.2023.109222>

Uttu A. J., Sallau M.S., Iyun O.R.A. and Ibrahim H. (2023B). *In vitro* antimicrobial studies of some major bioactive compounds isolated from *Strychnos innocua* (Delile) root bark. *Steroids*, 195, 109241. <https://doi.org/10.1016/j.steroids.2023.109241>



©2025 This is an Open Access article distributed under the terms of the Creative Commons Attribution 4.0 International license viewed via <https://creativecommons.org/licenses/by/4.0/> which permits unrestricted use, distribution, and reproduction in any medium, provided the original work is cited appropriately.